# Nonlinear imaging in optical path with linear negative and positive refractive-index media

Yonghua Hu[1] · Zhen Tang[1]

## Abstract

The nonlinear imaging in laser beam propagation is investigated theoretically under the circumstance that the linear media in the optical path model have arbitrary negative or positive refractive index. Based on the linear diffraction theory and thin-medium approximation, the propagation is solved analytically. Numerical simulation results obtained by split-step Fourier method are also presented. It is found that hot image can also be formed when either or both of the two linear media have negative refractive index, and that the intensity of hot image is closely related to the combination of refractive indices. The intensity of hot image is discussed in detail for different cases. Furthermore, it is found that the refractive indices of the linear media play important roles in image distance, resulting in that the hot image is no longer constrained in the conjugate plane of the scatterer.

## 1 Introduction

During the propagation of intense laser beams, they may encounter small-scale scatterers in optical path, such as scratch, dirt, dust, bubbles, or local imperfections in optical components. The scatterers will impose amplitude or phase modulation on the laser beams. As a result of the propagation of such modulated laser beams, intense hot image [1–4] (bright fringe or spot) of scatterer can be formed in the conjugate plane which is in the downstream area of a nonlinear medium slab with Kerr nonlinearity. This is a lens-less imaging process, and the effect is called nonlinear imaging or nonlinear holographic imaging [5]. In the typical conventional optical path of nonlinear imaging, the Kerr medium slab is between two free space (i.e., linear media with refractive index $n = 1$) areas, and it plays the role of a special lens in hot image formation. As an important effect in high-power laser systems, nonlinear imaging has drawn a lot of attention in the past decades. It has been found that, like self-phase modulation [6] or self-focusing [7], the physical origin of nonlinear imaging is the third-order nonlinearity in the nonlinear medium slab. For the hot image, its intensity is mainly determined by the modulation properties of the scatterer and the B-integral value of the optical path. Besides, the imaging properties are related to the envelope shape of incident beam [8], the properties of the Kerr medium [9], the structure of the optical path [10, 11], etc. When the incident beam is modulated by more than one scatterer, some other intense fringes can also be formed [12–14].

As a nonlinear effect, it is found that nonlinear imaging effect can be suppressed by inserting an extra spatial filter into the optical path [15] or using broadband background beams [16], which are at the cost of making the laser system more complicated. However, newly developed media often allow people to better govern and make use of known optical effects. In this respect, negative-index media (metamaterials) [17], also called left-handed media, have been developed rapidly in recent years [18–21] due to their very attractive optical properties unavailable in nature. The optics of negative-index media has brought people into a new stage for the understanding of some conventional optical phenomena [22, 23]. The properties of negative-index media also have an important influence on the nonlinear propagation of light. So far, some new propagation properties or phenomena have been discovered in some typical nonlinear optical effects [24–29], as well as the formation of hot image by a nonlinear negative-index medium slab [30]. Besides, it has been shown that negative-index media provide a new way to manipulate high-intensity laser field [31–33].

✉ Yonghua Hu
  huyh@hnust.cn

1 School of Computer Science and Engineering, Hunan University of Science and Technology, Xiangtan 411201, China

Unlike the case studied in Ref.[30], we noted that the propagation in the linear media of the whole optical path of nonlinear imaging is also critical. For these linear media, the nonlinear index is zero or small enough to be neglected. Thus, the nonlinear imaging in the linear negative-index medium case is worth studying. However, there is no literature about this so far. In this paper, we study the propagation of nonlinear imaging under the circumstance that the refractive index range of the linear media is extended to cover the negative value region. We will identify the conditions for the formation of hot image and show the special role the negative-index medium playing in nonlinear imaging. Our presentation is structured as follows. In Sect. 2, we present the propagation model. In Sect. 3, we present the analytical solution of the propagation, identify the different cases for the formation of hot image and derive the analytical expressions for the intensity and on-axis position of hot image. In Sect. 4, we demonstrate the formation of hot image and the basic nonlinear imaging properties by numerical simulation. Finally, in Sect. 5, we present our conclusions.

## 2 Model

The propagation is sketched in Fig. 1, where an intense laser beam propagates through the plane Ps, the first linear medium (LMa) and a conventional Kerr medium slab in turn, and then it propagates in the second linear medium (LMb). In this figure: there is a scatterer (dozens to hundreds of micrometers in size) in Ps; both LMa and LMb are either linear positive-index or negative-index medium; in LMb, the hot image of the scatterer will be formed in the plane Ph. In our presentation, we are mainly interested in revealing the basic properties of nonlinear imaging, so we assume that the linear media are homogeneous and isotropic.
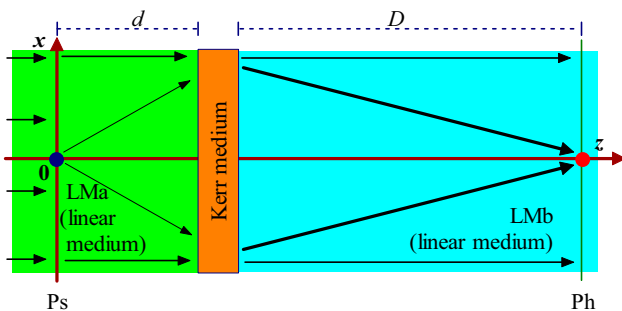


**Fig. 1** The schematic diagram of propagation model. Ps and Ph are the scatterer plane and the image plane, respectively. The circle dot in Ps represents a small-scale scatterer, and the circle dot in Ph represents the corresponding hot image bright spot formed downstream of the Kerr medium slab

For the small-scale scatterer in Ps, we assume that its complex amplitude transmittance can be expressed as $t_m = \tau_m \exp(ip_m)$. According to the Babinet principle, the overall complex amplitude transmittance of the plane Ps can be written as

$$t_0 = 1 - t_{m,c}, \tag{1}$$

where $t_{m,c}$ is the complementary amplitude transmittance of $t_m$. In what follows, we write the refractive indices of LMa and LMb as $n_a$ and $n_b$, respectively. If LMa or LMb is free space, we have $n_a = 1$ or $n_b = 1$.

## 3 Analytical analysis and formation of hot image

For analytical solution, we consider a plane wave incidence at $z = 0$ which can be normalized as $G = \exp[i(kz-\omega t)]$ with respect to its amplitude, and we define the normalized intensity as $I_r = |G|^2$. Under the far-field condition, the complex field amplitude at the incident surface of the nonlinear medium slab is given by

$$G(x_2, y_2) = G_L(x_2, y_2) + G_M(x_2, y_2), \tag{2}$$

where $G_M$ is the term for the scattered field and $G_L$ is the term for the background field. Under the far-field condition, we have

$$G_L(x_2, y_2) = \exp(-\alpha_a d/2) \exp(ik_a d), \tag{3}$$

and

$$G_M \approx n_a \exp(-\alpha_a d/2) \left[\exp(ik_a d)/(i\lambda d)\right] T_{m,c}\left(\frac{n_a x_2}{\lambda d}, \frac{n_a y_2}{\lambda d}\right), \tag{4}$$

where $k_a = 2\pi n_a/\lambda$ is the wavenumber in LMa, $\alpha_a$ is the attenuation constant of LMa at the wavelength $\lambda$, and $T_{m,c}$ is the Fourier transform of $t_{m,c}$.

The propagation of monochromatic beam in the conventional Kerr medium slab can be described by the nonlinear Schrödinger (NLS) equation

$$\frac{\partial G}{\partial z} = i\frac{1}{2k_0}\nabla_\perp^2 G + iB_s|G|^2 G, \tag{5}$$

where $\nabla_\perp^2 = (\partial^2/\partial x^2) + (\partial^2/\partial y^2)$, $k_0 = 2\pi n_0/\lambda$ is the wave number, $B_s = (k_0 n_2/n_0)|A_0|^2$ is the coefficient of the nonlinear item of the equation, $n_2 = (3/4)(\chi^{(3)}/n_0)$, $\chi^{(3)}$ is the third-order nonlinear susceptibility, and $A_0$ is the peak amplitude of the beam at $z = 0$. Under the thin-medium approximation, the diffraction term of Eq. (5) can be neglected. Then the complex field amplitude at the exit surface of the nonlinear medium can be given by

$$G(x_3, y_3) = G(x_2, y_2) \exp\left[iB_sL|G(x_2, y_2)|^2\right], \tag{6}$$

where $L$ is the thickness of the Kerr medium slab.

In LMb, the complex filed amplitude in the plane with a distance $D$ from the exit surface of the Kerr medium slab can be obtained by Fresnel diffraction integral as

$$G(x_4, y_4) = n_b \exp\left(-\alpha_b D/2\right)\left[\exp\left(ik_b D\right)/(i\lambda D)\right]\iint_\infty G(x_3, y_3)\exp\left(iK_4\right)dx_3 dy_3, \tag{7}$$

where $K_4 = \left(k_b/2D\right)\left[\left(x_4 - x_3\right)^2 + \left(y_4 - y_3\right)^2\right]$ and $\alpha_b$ is the attenuation constant of LMb at the wavelength $\lambda$.

Under the mean field approximation, the scattered wave at the incident surface of the Kerr medium can be viewed as perturbation, i.e., $|G(x_2, y_2)| \approx \exp(-\alpha_a d/2)$. Using the Taylor expansion formula under the far-field condition, we can rewrite the exponential part of Eq. (6) as

$$\exp\left(iB_sL\right)\left[1 + iB_sL\left(G_LG_M^* + G_MG_L^* + |G_M|^2\right)\right], \tag{8}$$

where * represents phase conjugation. Therefore,

$$G(x_4, y_4) \approx \frac{n_b}{i\lambda D}\exp\left[-(\alpha_a d + \alpha_b D)/2\right]\left(U_\alpha + U_\beta + U_\gamma + U_\delta\right)\exp\left[i(k_b D + B_sL)\right], \tag{9}$$

$$U_\alpha(x_4, y_4) = \iint_\infty \exp\left(iK_4\right)dx_3 dy_3, \tag{10}$$

$$U_\beta(x_4, y_4) = iB_sL\iint_\infty G_LG_M^* \exp\left(-i2\pi Q_4\right)dx_3 dy_3, \tag{11}$$

$$U_\gamma(x_4, y_4) = iB_sL\iint_\infty G_MG_L^* \exp\left(-i2\pi Q_4\right)dx_3 dy_3, \tag{12}$$

and

$$U_\delta(x_4, y_4) = iB_sL\iint_\infty |G_M|^2 \exp\left(-i2\pi Q_4\right)dx_3 dy_3, \tag{13}$$

where

$$Q_4 = \left[n_b x_4/(D\lambda)\right]x_3 + \left[n_b y_4/(D\lambda)\right]y_3. \tag{14}$$

It is easy to see from Eqs. (10) and (13) that $U_\alpha$ is the component for background field propagation and $U_\alpha = iD\lambda/n_b$, and that $U_\delta$ is the autocorrelation term of perturbation field $G_M$, which is much smaller than other terms and can be neglected. However, for $U_\beta$ and $U_\gamma$, according to Eqs. (11) and (12), the corresponding integrals depend on the values of $n_a$ and $n_b$.

According to Fig. 1, when the refractive index of the linear media is in the whole range of the number axis, there are four refractive index combination modes: (1) $n_a > 0$ and $n_b > 0$; (2) $n_a < 0$ and $n_b < 0$; (3) $n_a > 0$ and $n_b < 0$; and (4) $n_a < 0$ and $n_b > 0$. In what follows, we call the combination modes (1) and (2) "same refractive index sign case" (same-RIS case for short), and the combination modes (3) and (4) "opposite refractive index sign case" (opposite-RIS case for short). Besides, we use "free space case" to represent the conventional case where LMa and LMb are free space.

## 3.1 Same-RIS case

For the same-RIS case, we can see from Eq. (12) that $U_\gamma$ is the diffraction term for the complementary field propagation of the scattered filed. For $U_\beta$, under the condition

$$n_a/d = n_b/D, \tag{15}$$

we obtain from Eq. (11) that

$$U_\beta(x_4, y_4) = F_sB\lambda t_{m,c}^*\left(x_4, y_4\right)\exp\left(-\alpha_a d\right), \tag{16}$$

where $F_s = d/n_a$, $B = B_sL$ and it represents the B-integral value. When both LMa and LMb are free space, Eq. (16) indicates that a real image will be formed downstream the Kerr medium. This real image is the so-called hot image revealed in literatures (e.g., [1–4]). However, Eq. (16) also holds true when $n_a$ and $n_b$ are simultaneously negative. Thus, it can be inferred that hot image can be formed when both LMa and LMb have arbitrary negative refractive index value.

## 3.2 Opposite-RIS case

For the opposite-RIS case which is completely different from the conventional circumstances, it is easy to see from Eq. (11) that $U_\beta$ becomes the diffraction term for the propagation of the complementary field of the scattered filed. Will hot image form in this case? We noticed that we can turn to $U_\gamma$. Substituting Eqs. (3) and (4) into Eq. (12), under the condition

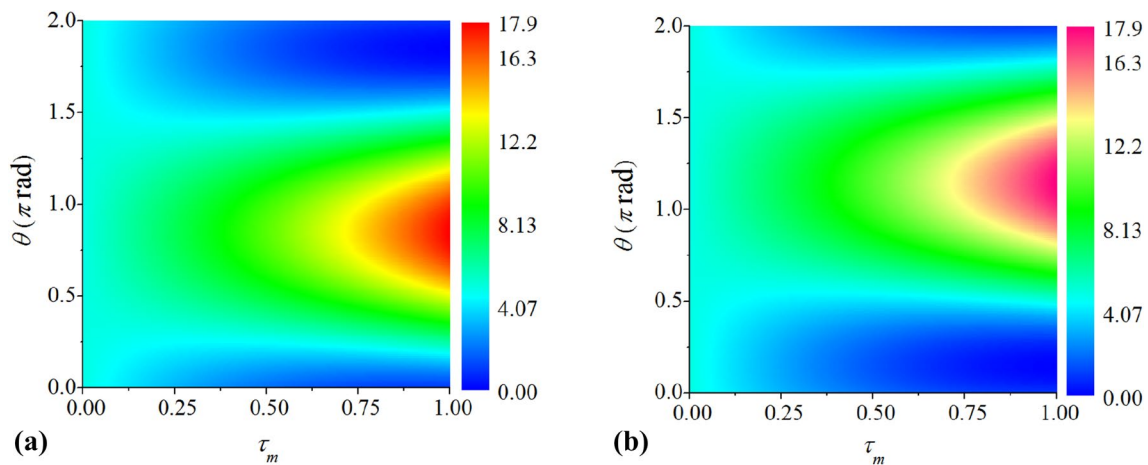$$|n_a|/d = |n_b|/D, \tag{17}$$

we obtain that

**Fig. 2** The relation between hot image intensity and the modulation properties of scatterer. $\theta = p_m/\pi$. **a** The same-RIS case, **b** the opposite-RIS case

$$U_\gamma(x_4, y_4) = -F_o \text{sgn}(n_a) B\lambda t_{m,c}(x_4, y_4) \exp(-\alpha_a d), \quad (18)$$

where $F_o = d/|n_a|$, "sgn" represents the operation of taking the sign value of refractive index and the result should be either 1 or −1. It is easy to see that Eqs. (17) and (18) are akin to Eqs. (15) and (16). This indicates that Eq. (18) holds true when either LMa or LMb is a negative-index medium and the other one's refractive index has the opposite sign. Thus, it can also be inferred that hot image will also be formed in LMb in the case where $\text{sgn}(n_a) = -\text{sgn}(n_b)$.

### 3.3 Properties of nonlinear imaging

According to the above-obtained results, we can further get the intensity in the beam spot area corresponding to the scatterer at the position predicted by Eq. (15) or Eq. (17)., Neglecting the diffraction term for the complementary field propagation of the scattered filed and $U\delta$, we have the complex filed amplitude as

$$G(x_4, y_4) \approx \left[1 - iBt_{m,c}^*(x_4, y_4) \exp(-\alpha_a d)\right] \exp\left[i(k_b D + B_s L) - (\alpha_a d + \alpha_b D)/2\right] \quad (19)$$

for the same-RIS case, and

$$G(x_4, y_4) \approx \left[1 - iBt_{m,c}(x_4, y_4) \exp(-\alpha_a d)\right] \exp\left[i(k_b D + B_s L) - (\alpha_a d + \alpha_b D)/2\right] \quad (20)$$

for the opposite-RIS case. Then we obtain the normalized intensity $I_h$, i.e., the maximum $|G|^2$ in the plane determined by Eq. (16) or Eq. (18), as: for the same-RIS case,

$$I_h = \left\{ \begin{array}{l} 1 + 2B\tau_m \sin(p_m) \exp(-\alpha_a d) \\ + [1 + \tau_m^2 - 2\tau_m \cos(p_m)] B^2 \exp(-2\alpha_a d) \end{array} \right\} \exp\left[-(\alpha_a d + \alpha_b D)\right]; \quad (21)$$

for the opposite-RIS case,

$$I_h = \left\{ \begin{array}{l} 1 - 2B\tau_m \sin(p_m) \exp(-\alpha_a d) \\ + [1 + \tau_m^2 - 2\tau_m \cos(p_m)] B^2 \exp(-2\alpha_a d) \end{array} \right\} \exp\left[-(\alpha_a d + \alpha_b D)\right]. \quad (22)$$

From the above analysis for both the same-RIS and opposite-RIS cases, we can see that, whatever the signs of the refractive indices of the linear media are, hot image can be formed in LMb when the condition given by Eq. (17) is satisfied. Equations (21) and (22) show that $I_h$ is the function of the complex amplitude transmittance of scatterer and the B-integral in the Kerr medium. However, we note that the second terms of Eqs. (21) and (22) have opposite signs. This indicates that $I_h$ of the two cases are different from each other when other parameters are the same. To show the difference between the two cases, we take $B = 2$ rad for an example. Besides, we neglect the attenuation in the media, i.e., set $\alpha_a = \alpha_b = 0$, in order to reflect the basic nonlinear imaging properties. The corresponding quantitative relation between $I_h$ and $\tau_m$ and $p_m$ is shown in Fig. 2. It is easy to see that the variation of $I_h$ with either $\tau_m$ and $p_m$ is great.

To better illustrate the difference between the two cases, we show the variation of hot image intensity with the amplitude transmittance and the phase modulation depth in Fig. 3. Figure 3a shows that, at the phase modulation depth $p_m = 0.5\pi$ rad, as $\tau_m$ increases, the $I_h$ in the opposite-RIS case keeps relatively small, but the $I_h$ in the same-RIS case increases almost monotonically, and the largest difference between them is at $\tau_m = 1$ and is about eight times the incident beam intensity. In the aspect of phase modulation depth, it is easy to see from Fig. 3b that the two curves are symmetrical to each other at $p_m = \pi$ rad.

For the free space case investigated in literatures so far, we note that the relation between image and object distances is $D = d$. However, for the cases considered in this paper, we can easily obtain from Eq. (17) that

$$D = \left( |n_b|/|n_a| \right) d. \tag{23}$$

This indicates that, for a certain object distance, the image distance is in inverse proportional to $|n_a|$ but is proportional to $|n_b|$. For example, if LMb is free space ($n_b = 1$) and $d = 1.0$ m, then $D$ is 5.0 m for $n_a = -0.2$.

Equation (23) reveals an important law of the nonlinear imaging cases discussed in this paper. Because the refractive index value of a negative-index medium can be artificially designed [theoretically ($-\infty, 0$)], this law means that the position of hot image plane can be effectively planned, such as outside of an area contains optical elements or at a position in need. In virtue of this, the structure design of optical path can be relieved from the adverse effect of nonlinear imaging to a great extent. In addition, the purpose people studying nonlinear imaging so far is to suppress it. However, every coin has two sides. Based on this law, we can anticipate that the positive value of nonlinear imaging will be gradually explored.

## 4 Numerical simulation and discussion

In this section, we solve the propagation with numerical simulation by using the standard split-step Fourier method based on the fast Fourier transform algorithm. We assume that the incident beam is a flat-topped Gaussian beam whose super-Gaussian order is $m$ and the radius at the $1/e$-intensity point is $r_0$:

$$G(x_0, y_0) = \exp \left[ -\frac{1}{2} \left( \frac{x_0^2 + y_0^2}{r_0^2} \right)^m \right]. \tag{24}$$

Unless noted, the default parameters are as follows: for the incident beam, $\lambda = 1053$ nm, $m = 6$, $r_0 = 5$ mm. For the small-scale scatterer, it is an opaque wirelike one ($t_{m,c} = 1$) and is long enough to run through the beam spot in the $y$ direction and is centered at $x = 0$, the width $w$ is 200 μm. For the case LMa or LMb is negative-index medium, $n_a = -1$ or $n_b = -1$. For the Kerr medium slab, $n_0 = 1.5$, $L = 5$ mm, $B_s = 400$ rad/m for $B = 2$ rad. Besides, $d$ is set as 1.0 m. Under these default parameters, the on-axis position of the image plane is at $z = 2.005$ m according to Eq. (23). For the incident beam spot, the sampling window size is $60 \times 60$ mm$^2$, the beam center is at the center of this window, and the sample point number is 8192 for each dimension. The step length in the split-step simulation is 50 mm in LMa and LMb and 1 mm in the Kerr medium slab. Besides, the diffraction term in Eq. (5) is ignored because of the thin-medium approximation.

We traced the beam maximum intensity $I_m$ and the intensity distribution of the beam spot in numerical simulation. For the above-mentioned (2), (3) and (4) refractive index combination modes of LMa and LMb, the corresponding evolution of $I_m$ is shown in Fig. 4 by curves (a), (b) and (c). This figure shows that each curve has an outstanding peak

**Fig. 3** The variation of hot image intensity with **a** $\tau_m$ at $p_m = 0.5\pi$ rad and **b** $\theta$ ($\theta = p_m/\pi$) at $\tau_m = 0.9$. (i) $I_h$ for the same-RIS case and (ii) $I_h$ for the opposite-RIS case
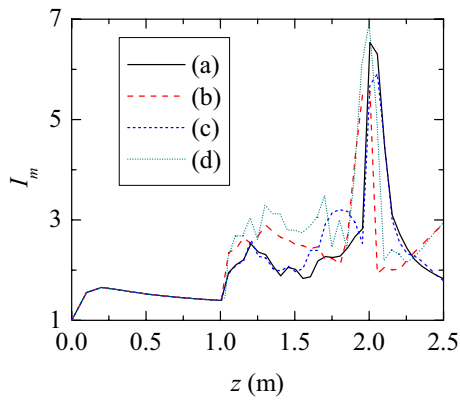


(a)



(b)
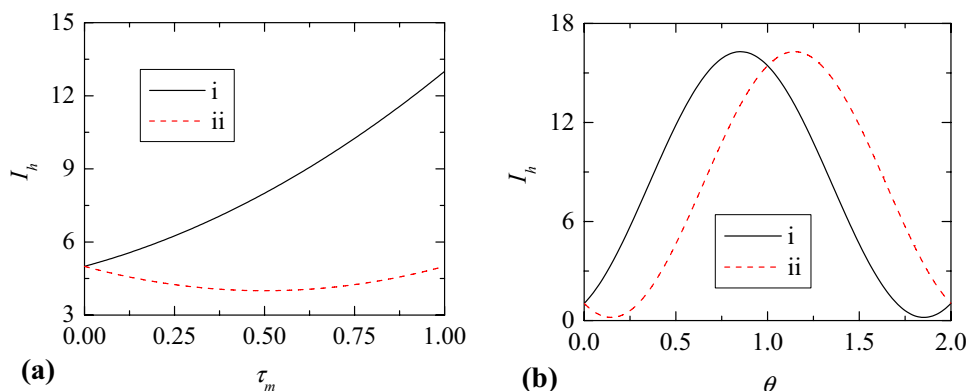
**Fig. 4** The variation of $I_m$ with propagation distance. **a** LMa and LMb are negative-index media. **b** LMa is negative-index medium and LMb is free space. **c** LMa is free space and LMb is negative-index medium. **d** LMa is negative-index medium and LMb is free space, $L = 50$ mm

and all the peaks are at about $z = 2.0$ m. For these results, we note that the effect of diffraction in the Kerr medium is neglected. However, when the thickness of the Kerr medium is large enough, the effect of diffraction in the Kerr medium may become important. To show this, we take the case (3), i.e., LMa is negative-index medium and LMb is free space, for example. We set $L = 50$ mm (so $B_s = 40$ rad/m for $B = 2$ rad) and consider the diffraction in the Kerr medium in numerical simulation. The evolution of $I_m$ is shown by the short-dotted curve (d) of Fig. 4. Comparing curves (b) and (d), it is easy to see that the peak for $L = 50$ mm is obviously higher than that of curve (b).

The beam intensity distributions corresponding to the peaks of curves (a), (b) and (c) in Fig. 4 are shown in Fig. 5. It is easy to see from Fig. 5 that, for each refractive index combination mode, there is a bright fringe whose in-beam position is the same as that of the scatterer, and this fringe is the most intense one in the whole beam spot. This is the same as the free space case and it shows that hot images are indeed formed when one of the linear medium is or both
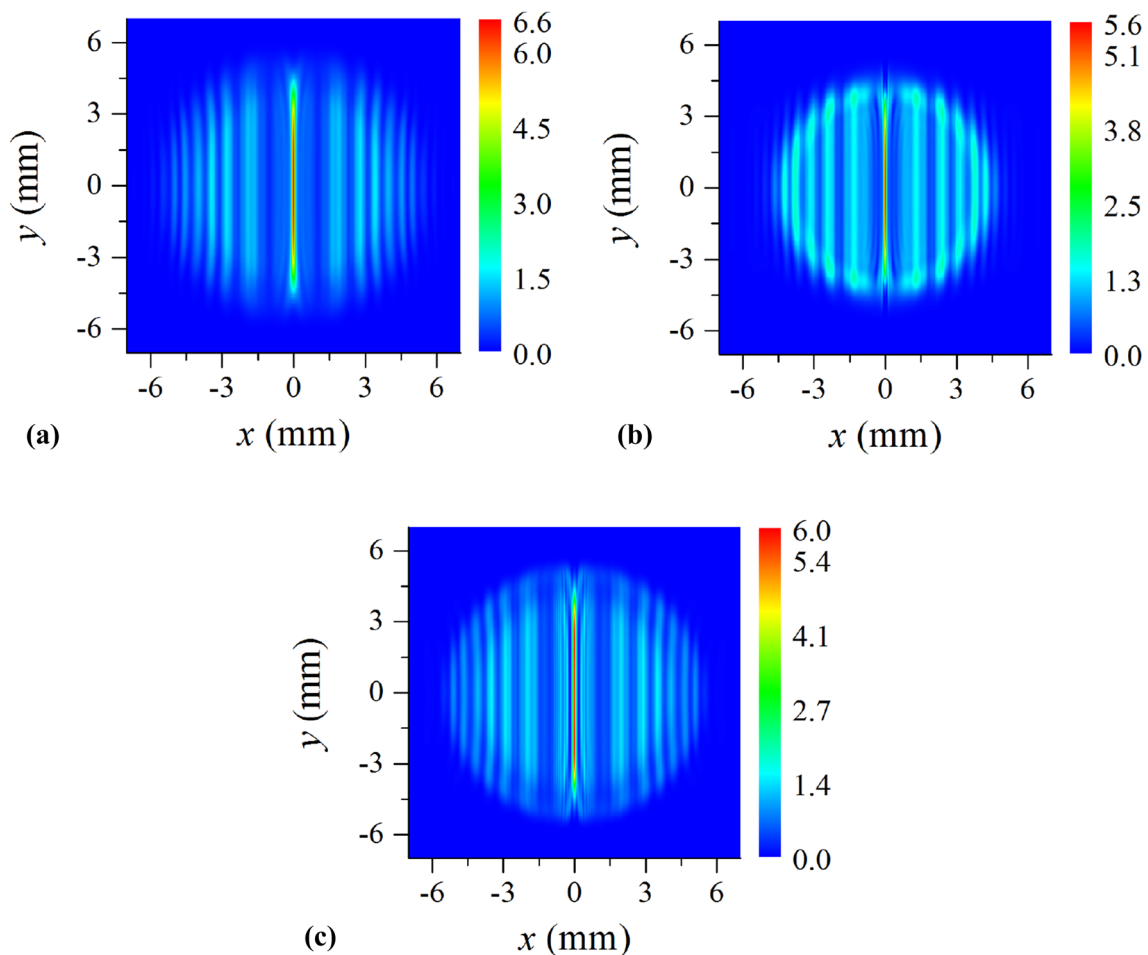


**(a)**



**(b)**



**(c)**

**Fig. 5** Normalized beam intensity spot in the hot image plane. **a** LMa and LMb are negative-index media. **b** LMa is negative-index medium and LMb is free space. **c** LMa is free space and LMb is negative-index medium
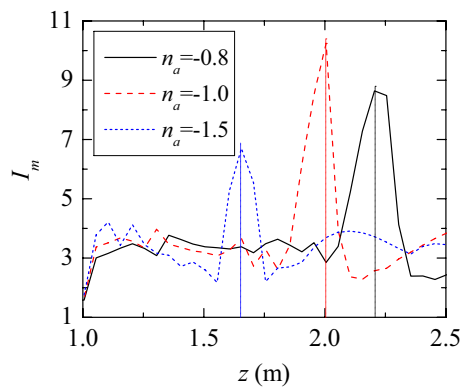
**Fig. 6** Evolution of $I_m$ at different values of $n_a$. LMa is negative-index medium and LMb is free space

linear media are negative-index medium. So, we also call such intense bright fringes hot images. In what follows, we use the maximum intensity $I_h$ in the hot image plane to represent the hot image intensity. According to Figs. 4, 5, it is clear that $I_h$ is about six times the incident beam intensity. This is basically in accordance with the approximate analytical results given by Eqs. (21) and (22). Besides, for the image distances, they are very close to the value 1.0 m given by Eq. (23) and that in the corresponding free space case under the default parameters.

To demonstrate the image distance law shown by Eq. (23), we assume that LMa is a negative-index medium and investigate the nonlinear imaging propagation at three different $n_a$ values − 0.8, − 1.2 and − 1.5. The corresponding evolution curves of $I_m$ starting from $z = 1.0$ m are shown in Fig. 6. For the curves shown in Fig. 6, the amplitude transmittance and phase modulation depth are 0.6 and $(3/4)\pi$ rad, respectively. It is easy to see that as $|n_a|$ decreases, the peak of the curve gets away from the nonlinear medium. The on-axis position of the maximums of $I_m$ corresponding to three $n_a$ values − 0.8, − 1.2 and − 1.5 are approximately at 2.205, 2.005 and 1.655 m (see positions marked by the vertical dotted lines), respectively. This is in good accordance with Eq. (23).

We note that the above result of image distance applies to all the four refractive index combination modes. Thus, the effect shown by Fig. 6 is not limited to the case where LMa is a linear negative refractive index medium.

## 5 Conclusions

In conclusion, we have investigated the propagation properties of nonlinear imaging in an optical path with linear negative-index media through analytical analysis and computer numerical simulation. We have proved that the hot image of small-scale scatterer can be formed when any of the two

linear media before and behind the Kerr medium slab has either positive or negative refractive index. According to the refractive index sign combination mode, the formation of hot image can be divided into two general cases, i.e., the same-RIS case and the opposite-RIS case. The effect of the scatterer's phase modulation depth on hot image intensity in the former is opposite to that in the latter. Moreover, the image distance is proportional to the ratio of the refractive indices of the two linear media. This makes nonlinear imaging to have an adjustable focal length, or say the image distance becomes a parameter that can be preset. Thus, using negative-index medium is an effective way to reduce the threat of hot image on optical elements in high-power laser systems, and the application of nonlinear imaging becomes explorable for some appropriate circumstances.

## Compliance with ethical standards

**Conflict of Interest** The authors declare that they have no conflict of interest.

## References

1. J.T. Hunt, K.R. Manes, P.A. Renard, Appl. Optics **32**(30), 5973–5982 (1993)
2. W.H. Williams, K.R. Manes, J.T. Hunt, P.A. Renard, D. Milam, D. Eimerl, ICF Quart. Rep. **6**, 7–14 (1996)
3. C.C. Widmayer, D. Milam, S.P. DeSzoeke, Appl. Optics **36**(36), 9342–9347 (1997)
4. L. Xie, J. Zhao, J. Su, F. Jing, W. Wang, H. Peng, Acta Physics Sin. **53**, 2175–2179 (2004)
5. S.G. Garanin, I.V. Epatko, R.I. Istomin, L.V. L'vov, A.A. Malyutin, R.V. Serov, S.A. Sukharev, Appl. Optics **50**(21), 3733–3741 (2011)
6. A.A. Drozdov, S.A. Kozlov, A.A. Sukhorukov, Y.S. Kivshar, Phys. Rev. A **86**(5), 053822 (2012)
7. Y. Cheng, H. Xie, Z. Wang, G. Li, B. Zeng, F. He, W. Chu, J. Yao, L. Qiao, Phys. Rev. A **92**(2), 023854 (2015)
8. Y. Wang, Y. Hu, S. Wen, K. You, X. Fu, Acta Phys. Sin. **56**, 5855–5861 (2007)
9. Y. Wang, J. Deng, L. Chen, S. Wen, K. You, Chin. Phys. Lett. **26**(2), 024205 (2009)
10. T. Peng, J. Zhao, D. Li, Opt. Laser. Eng. **49**(7), 972–978 (2011)
11. Y. Wang, S. Wen, K. You, Z. Tang, J. Deng, L. Zhang, D. Fan, Appl. Optics **47**(30), 5668–5681 (2008)
12. Y. Hu, G. Li, L. Zhang, W. Huang, S. Chen, Opt. Express **23**(24), 30878–30890 (2015)
13. Y. Hu, X. Jie Huang, JXu Peng, J. Opt. Soc. Am. B **30**(2), 349–354 (2013)
14. J. Zhou, D. Li, Appl. Opt. **58**(2), 446–453 (2019)
15. Y. Zhang, J. Zhang, Z. Jiao, M. Sun, D. Liu, J. Zhu, Optik **126**, 1209–1212 (2015)

16. Y. Hu, Y. Wang, S. Wen, D. Fan, Chin. Phys. B **19**(11), 114207 (2010)

17. J. Yao, Z.W. Liu, Y.M. Liu, Y. Wang, C. Sun, G. Bartal, A.M. Stacy, X. Zhang, Science **321**(5891), 930–930 (2008)

18. S. Zhou, S. Townsend, Y.M. Xie, X. Huang, J. Shen, Q. Li, Opt. Lett. **39**(8), 2415–2418 (2014)

19. S. Xiao, V.P. Drachev, A.V. Kildishev, X. Ni, U.K. Chettiar, H.K. Yuan, V.M. Shalaev, Nature **466**, 735–738 (2010)

20. S. Jahani, Z. Jacob, Nat. Nanotechnol. **11**, 23–36 (2016)

21. Y. Liang, Z. Yu, N. Ruan, Q. Sun, T. Xu, Opt. Lett. **42**(16), 3239–3242 (2017)

22. T. Xu, A. Agrawal, M. Abashin, K.J. Chau, H.J. Lezec, Nature **497**, 470–474 (2013)

23. G. Rosenblatt, M. Orenstein, Phys. Rev. A **95**(5), 053857 (2017)

24. L. Zhang, X. Dai, Y. Xiang, S. Wen, Appl. Phys. B **121**(4), 465–472 (2015)

25. K. Popov, S.A. Myslivets, T.F. George, V.M. Shalaev, Opt. Lett. **32**(20), 3044–3046 (2007)

26. S. Lan, L. Kang, D.T. Schoen, S.P. Rodrigues, Y. Cui, M.L. Brongersma, W. Cai, Nat. Mater. **14**(8), 807–811 (2015)

27. A. Joseph, K. Porsezian, Phys. Rev. A **81**(2), 023805 (2010)

28. N. Raza, Indian J. Phys. **93**, 657–663 (2019)

29. Y. Hu, S. Wen, Y. Wang, D. Fan, Opt. Commun. **281**(9), 2663–2669 (2008)

30. Y. Hu, Y. Li, J. Yuan, Z. Tang, H. Lu, Opt. Commun. **450**, 122–129 (2019)

31. N. Segal, S. Keren-Zur, N. Hendler, T. Ellenbogen, Nat. Photonics **9**, 180–184 (2015)

32. Y. Hu, J. Zhou, J. Mod. Optic. **57**(1), 43–50 (2010)

33. J. Zhang, Y. Xiang, S. Wen, Y. Li, J. Opt. Soc. Am. B **31**(1), 45–52 (2014)